Journal of Medicinal Chemistry

Article

pubs.acs.org/jmc

Multitarget Drug Discovery for Tuberculosis and Other Infectious Diseases

Kai Li,[†,&] Lici A. Schurig-Briccio,[‡,&] Xinxin Feng,[†,&] Ashutosh Upadhyay,[§] Venugopal Pujari,[§] Benoit Lechartier,[∥] Fabio L. Fontes,[§] Hongliang Yang,[§] Guodong Rao,[†] Wei Zhu,[⊥] Anmol Gulati,[†] Joo Hwan No,[¶] Giovana Cintra,[¶] Shannon Bogue,[‡] Yi-Liang Liu,[⊥] Katie Molohon,[□] Peter Orlean,[□] Douglas A. Mitchell,[†,□,▽] Lucio Freitas-Junior,[¶] Feifei Ren,[#] Hong Sun,[#] Tong Jiang,[#] Yujie Li,[#] Rey-Ting Guo,[#] Stewart T. Cole,[∥] Robert B. Gennis,[†,‡] Dean C. Crick,[§] and Eric Oldfield*[,†,⊥]

[†]Department of Chemistry, University of Illinois at Urbana−Champaign, 600 South Mathews Avenue, Urbana, Illinois 61801, United States

[‡]Department of Biochemistry, University of Illinois at Urbana−Champaign, 600 South Mathews Avenue, Urbana, Illinois 61801, United States

[§]Department of Microbiology, Immunology and Pathology, Colorado State University, 200 West Lake Street, Fort Collins, Colorado 80523, United States

[∥]Global Health Institute, École Polytechnique Fédérale de Lausanne, Lausanne, Switzerland

[⊥]Center for Biophysics and Computational Biology, University of Illinois at Urbana−Champaign, 607 South Mathews Avenue, Urbana, Illinois 61801, United States

[¶]Institut Pasteur Korea, Sampyeong-dong 696, Bundang-gu, Seongnam-si, Gyeonggi-do, Korea

[□]Department of Microbiology, University of Illinois at Urbana−Champaign, 601 South Goodwin Avenue, Urbana, Illinois 61801, United States

[▽]Institute for Genomic Biology, University of Illinois at Urbana−Champaign, 1206 West Gregory Drive, Urbana, Illinois 61801, United States

[#]Industrial Enzymes National Engineering Laboratory, Tianjin Institute of Industrial Biotechnology, Chinese Academy of Sciences, Tianjin 300308, China

Supporting Information

ABSTRACT: We report the discovery of a series of new drug leads that have potent activity against *Mycobacterium tuberculosis* as well as against other bacteria, fungi, and a malaria parasite. The compounds are analogues of the new tuberculosis (TB) drug SQ109 (**1**), which has been reported to act by inhibiting a transporter called MmpL3, involved in cell wall biosynthesis. We show that **1** and the new compounds also target enzymes involved in menaquinone biosynthesis and electron transport, inhibiting respiration and ATP biosynthesis, and are uncouplers, collapsing the pH gradient and membrane potential used to power transporters. The result of such multitarget inhibition is potent inhibition of TB cell growth, as well as very low rates of spontaneous drug resistance. Several targets are absent in humans but are present in other bacteria, as well as in malaria parasites, whose growth is also inhibited.

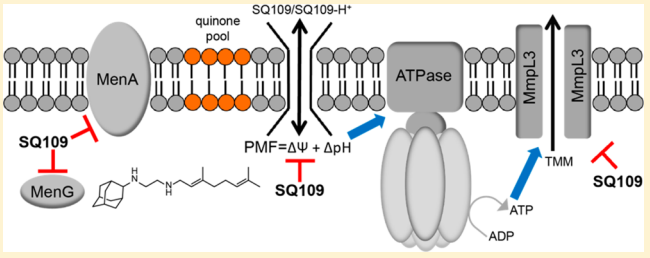

INTRODUCTION

Antibiotic resistance is a public health problem that, arguably, has the potential to destroy the efficacy of all antibiotics in the next 10−20 years.[1,2] There is, therefore, an urgent need for new drugs, especially ones that might be more "resistance-resistant". One possible approach to achieving this goal is to move away from targeting the direct killing of pathogens to inhibiting their virulence, because this might lead to a decreased "life or death" pressure on the organism to develop resistance.[3] A second approach would be to develop more drugs that target pathogen cell membranes. An example of this type of drug would be the antifungal amphotericin,[4] which functions by binding to ergosterol (which is not present in human cell membranes). A third and well-known approach is to employ combination therapies,[5] although the problems associated with finding two new drugs active against two new targets are clearly significant. A fourth approach is to use "multitargeting" or "polypharma-

Received: January 24, 2014
Published: February 25, 2014

cology" in which a single drug has more than one target.[6,7] This could involve "series inhibition", in which targets would be in the same metabolic pathway (Figure 1, left), "parallel inhibition", in which the targets would be unrelated but an inhibitor might mimic a common substrate or would affect, for example, a membrane function (Figure 1, middle), or "network inhibition", in which many targets in series and/or in parallel could be involved (Figure 1, right). While challenging, many drugs that have been effective in monotherapy do in fact have multiple targets[6] while single-target drugs (many of which are used in treating tuberculosis) are often only effective in combination therapies.

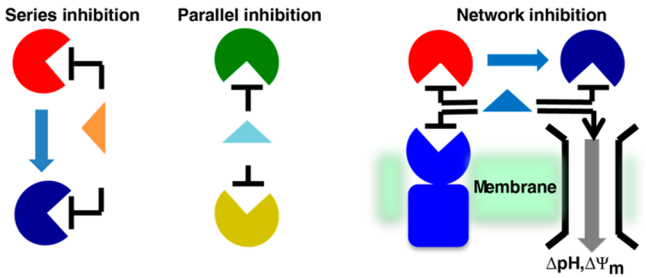

Figure 1. Series (in the same metabolic pathway), parallel (unrelated pathways or DNA/membrane targets), or network (series and parallel target) inhibition.

In this work, we consider the mechanism(s) of action of the new antituberculosis drug **1** (Chart 1), currently in phase II clinical trials.[8] This drug candidate appeared of interest because it contains a C_{10} isoprenoid (geranyl) side chain together with a strongly basic (ethylenediamine) fragment, a likely cationic center, suggesting that it might act as a carbocation isostere for a transition state/reactive intermediate in isoprenoid biosynthesis[9] and, as with other inhibitors of isoprenoid biosynthesis, it might be involved in multitargeting.[10] **1** was developed in a synthesis/screening program[11] in which ~64 000 ethylenediamine analogues of the antituberculosis drug ethambutol (**2**) were synthesized. **1** was ~4× more active than any of the other leads developed, having a minimum inhibitory concentration (MIC) of ~0.7−1.56 μM against *M. tuberculosis* (H37Rv, Erdman, and drug-resistant strains), and insights into its mode of action recently became available when the target of SQ109 was proposed[12] to be MmpL3, a trehalose monomycolate (TMM) transporter, an essential membrane protein that transports TMM into the cell envelope. This conclusion was based on the observation that several *M. tuberculosis* mutants produced via serial passage with several **1**-like inhibitors had mutations in the *mmpL3* gene and cross-resistance to **1**, although these latter effects were rather small.[12] More intriguingly, no spontaneous resistant mutants were obtained when using **1**, suggesting the possibility of multiple targets.[12,13] That idea is supported by the observation that **1** also has activity against other bacteria, e.g., *Helicobacter pylori*[14] as well as against the yeast *Candida albicans*,[15] neither of which possess the *mmpL3* gene, suggesting again that other **1** targets are harbored by these organisms and, potentially, by *M. tuberculosis*.

In this work, we synthesized a series of analogues of **1** in which we varied the adamantane headgroup and the ethylenediamine linker (varying the possible charge centers), Chart 1. All compounds were screened against a panel of bacteria (*M. tuberculosis*, *M. smegmatis*, *Escherichia coli*, *Staphylococcus aureus*, and *Bacillus subtilis*), two yeasts (*Saccharomyces cerevisiae* and *Candida albicans*), a malaria parasite (*Plasmodium falciparum*), and a human cell line (MCF-7), to establish antibacterial, antifungal and antimalarial structure−activity relationships and to assess mammalian cell toxicity. In addition, we investigated a subset of compounds for activity against a series of putative targets, isoprenoid biosynthesis enzymes, in addition to investigating the effects of these compounds on respiration, ATP synthesis, and the proton motive force (PMF).

RESULTS AND DISCUSSION

Only One Cationic Center Is Needed for Potent Activity in Mycobacteria. To investigate which features contribute to the activity of **1** against a broad range of organisms, we synthesized **1** and the 11 analogues (**3**−**13**) shown in Chart 1 in which the ethylenediamine linker was replaced by ethanolamine, choline, propanolamine, ethylene glycol, or glycolic amide moieties (providing linkers with potentially 0, 1, or 2 positive charges), as well several "head group" analogues in which the adamantyl group was varied. The geranyl "side chain" was kept constant. Full synthesis and characterization details are given in the Supporting Information. As expected, **1** had potent activity against *M. tuberculosis* with an MIC of ~0.1−0.2 μg/mL (Table 1). Interestingly, the *N*-geranyl ethanolamines **3** and **13** were more potent (MIC values as low as 0.02−0.05 μg/mL), indicating that the presence of two nitrogens was not essential for activity. The *O*-geranyl ethanolamine derivative (**4**) had activity similar to that of **1** (~0.2 μg/mL), Table 1. With the *N*-geranyl ethanolamines (**3**, **13**), activity was about 30-fold higher than with ethambutol (**2**). The ethylene glycol (**5**) was far less active (50 μg/mL), as was the glycolic amide **9** (12 μg/mL). Thus, the most active compounds all contain one strongly basic nitrogen in the linker region, with most activity being found with the two *N*-geranyl

Chart 1. Structures of Compounds Investigated

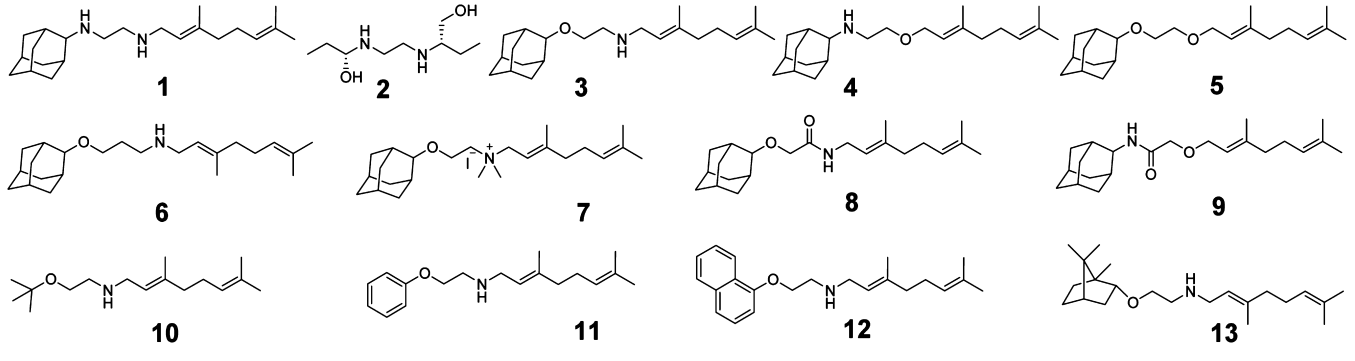

dx.doi.org/10.1021/jm500131s | J. Med. Chem. 2014, 57, 3126−3139

Table 1. Inhibition by 1 and Analogues of *M. tuberculosis* (Mt), *M. smegmatis* (Ms), *S. aureus* (Sa), *B. subtilis* (Bs), *E. coli* (Ec), *S. cerevisiae* (Sc), *C. albicans* (Ca), *P. falciparum* (Pf), and Human (MCF-7) Cell Growth

	Mt[a]	Ms[a]	Sa[a]	Bs[b]	Ec[b]	Sc[b]	Ca[b]	Pf[b]	MCF-7[b]
1	0.1−0.2 (0.3−0.6)	3.1(9.4)	>120(364)	7.6(23)	2.8(8.5)	1.1(3.3)	3.3(10)	1.0(3.0)	6.0(18)
2	2(9.8)[c]	1(4.9)[d]	–	–	–	–	–	–	–
3	0.02−0.05 (0.06−0.15)	1.6(4.8)	8(24)	16(48)	2.8(8.5)	1.8(5.4)	12(36)	0.79(2.4)	10(30)
4	0.19(0.57)	6.2(19)	>120(362)	>66(199)	4.3(13)	>33(100)	>66(199)	0.93(2.8)	112(338)
5	50(150)	>50(150)	>64(193)	>66(199)	>332(1000)	>332(1000)	>66(198)	7.9(24)	73(220)
6	1.6(4.6)	6.2(18)	8(23)	3.0(8.7)	2.3(6.7)	2.7(7.8)	6.5(19)	0.83(2.4)	3.4(9.8)
7	0.78(1.6)	12(24)	8(16)	4.2(8.6)	37(76)	15(31)	18(37)	0.08(0.16)	3.2(6.5)
8	0.78(2.2)	6.2(18)	>120(345)	>69(200)	>345(1000)	>69(200)	>69(200)	6.2(18)	12(35)
9	12(34)	25(72)	>120(348)	17(49)	>345(1000)	>69(200)	>69(200)	3.8(11)	9.3(27)
10	6.2(24)	50(198)	>16(63)	>50(198)	>126(498)	44(174)	>50(198)	3.2(13)	45(178)
11	6.2(23)	12(44)	32(117)	17(62)	60(220)	3.0(11)	20(74)	14(51)	6.3(23)
12	6.2(19)	12(37)	8(25)	2.4(7.4)	15(46)	3.7(11)	12(37)	>100(309)	7.1(22)
13	0.05(0.15)	1.6(4.8)	8(24)	1.8(5.4)	12(36)	0.89(2.7)	6.3(19)	2.0(6.0)	1.3(3.9)

[a]MIC, μg/mL, values in parentheses are in μM. [b]IC_{50}, μg/mL, values in parentheses are in μM. [c]Reference 16. [d]Reference 17.

ethanolamines **3** and **13** (Table 1), with **3** being ∼4−5 times more active than that of **1**.

We then tested all 12 compounds against *M. smegmatis*. The results (Table 1) show that overall activity against *M. smegmatis* is less than that observed against *M. tuberculosis*, as can also be seen in the "heat map" shown in Figure 2A. There is, however, a very high correlation coefficient (R^2 = 0.9, Figure 2B) between the pIC_{50} (= $-\log_{10}$ IC_{50}) values for *M. tuberculosis* and *M. smegmatis*, indicating a similar mechanism of action, leading to our use of *M. smegmatis* in several mechanism of action studies, as described below.

The Cationic Inhibitors Exhibit Broad Antibacterial, Antifungal, and Antimalarial Activity. All 12 compounds (**1**, **3**−**13**) were then tested against three other bacteria: *S. aureus*, *B. subtilis*, and *E. coli*, Table 1. With *S. aureus* (the methicillin-resistant *S. aureus* (MRSA) USA300 strain), **1** itself had little activity; however, the *N*-geranyl ethanolamines **3**, **12**, **13** and the *N*-geranyl propanolamine **6** all had MIC values of ∼8 μg/mL, while the other analogues were much less active (MIC > 32 μg/mL). A similar pattern of activity was seen against *B. subtilis*, with the three ethanolamines (**6**, **12**, **13**) exhibiting the highest levels of activity. In addition, unlike with *S. aureus*, **1** itself had activity (7.6 μg/mL, Table 1). With *E. coli*, **1**, the *N*-geranyl ethanolamine (**3**) and the *N*-geranyl propanolamine (**6**) were all quite active, with IC_{50} values of ∼2−3 μg/mL, Table 1. Moreover, there was a modest correlation (R^2 = 0.5) between the *M. tuberculosis* (or *M. smegmatis*) pMIC values and those found with *E. coli*, Figure 2B. These results again indicate that at least one basic amine, most likely a cationic center, is required for best activity; plus, there must be a target or targets other than MmpL3 in *E. coli* because the *mmpL3* gene is absent in this organism. Bioinformatics searches did locate uncharacterized *mmpL3*-like genes in *S. aureus* and *B. subtilis*, but it remains to be seen if the corresponding proteins are targeted by our compounds.

We next tested all 12 compounds (**1**, **3**−**13**) for activity against *S. cerevisiae* and *C. albicans*. As can be seen in Table 1 and Figure 2A, **1** and the ethanolamines **3**, **6**, **11**, and **13** had activity in the 1−3 μg/mL range, with **1** and **13** being the most potent, having an IC_{50} ∼ 1 μg/mL. With *C. albicans*, **1** was most active, followed by the ethanolamines **3** and **13**. Not unexpectedly, there was a high correlation between the pIC_{50} values seen between *S. cerevisiae* and *C. albicans* (R^2 = 0.8; Table 1 and Figure 2B). A modest correlation between the pIC_{50} values for the yeasts and *E. coli* or *B. subtilis* is also apparent (R = 0.6−0.7, Figure 2B), suggesting the possibility of target conservation between fungi and bacteria. Because a recognizable *mmpL3* gene is absent in the fungi, these results again indicate an alternate target or targets. These results also lead to the idea that there could be additional targets in *M. tuberculosis*, which would help explain the very low MIC values observed and the inability to induce resistance via serial passage, as noted by Tahlan et al.,[12] although multiple-targeting does not necessarily guarantee improved potency. The results with the bacteria and fungi then suggested the possibility that the growth of other organisms (protozoa) might also be inhibited by **1** or its analogues.

To evaluate antiprotozoal activity we screened all 12 compounds (**1**, **3**−**13**) against the intraerythrocytic form of the malaria parasite, *Plasmodium falciparum*. As can be seen in Table 1, **1** had a ∼1 μg/mL activity against *P. falciparum*, and the three ethanolamines (**3**, **4**, and **6**) also had good activity. As viewed on the heat map (Figure 2A), inhibition of *M. tuberculosis* cell growth is strongest but is followed by *P. falciparum* (in the intraerythrocytic assay) and in each case where there is activity against *P. falciparum* (**2**, **3**, **4**, **6**, **7**), the inhibitors (Chart 1) are expected to carry a +1 charge, as with the best *M. tuberculosis* growth inhibitors. When compared to growth inhibition results with a human cell line (MCF-7; Table 1), we see that activity against the human cells is much weaker than against *P. falciparum* and, of course, against *M. tuberculosis*. We calculate a therapeutic index (TI), defined as:

$$\mathrm{TI} = \frac{IC_{50}(\text{human cell line})}{IC_{50}(\text{pathogen})}$$

of ∼18 for **1** against *P. falciparum* and ∼40 for **3**, while for *M. tuberculosis* we find TI = 120 (**1**) and TI = 900 (**3**), suggesting that these and related analogues may also be promising *P. falciparum* drug leads. Because the human cell growth assays are carried out in the presence of 10% fetal bovine serum (FBS), we tested three of the most active compounds (**1**, **3**, **13**) against *E. coli* in the presence or absence of 10% FBS. There was only a 1.6 ± 0.07× increase in the IC_{50}, meaning that, as expected, serum binding is small and quite similar for each of these compounds. We next sought to explore what the additional targets for these compounds might be in cells that lack MmpL3.

dx.doi.org/10.1021/jm500131s | J. Med. Chem. 2014, 57, 3126−3139

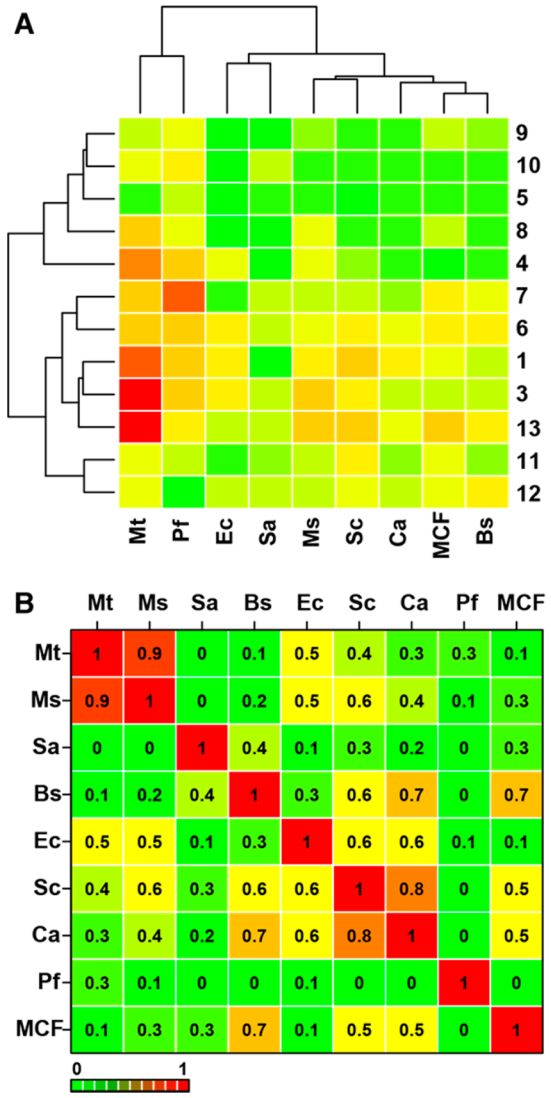

Figure 2. Inhibition of cell growth for *M. tuberculosis* (Mt), *M. smegmatis* (Ms), *S. aureus* (Sa), *B. subtilis* (Bs), *E. coli* (Ec), *S. cerevisiae* (Sc), *C. albicans* (Ca), *P. falciparum* (Pf), and a human cell line (MCF-7) by **1**, **3**–**13**. (A) Heat map. Red = strong inhibition; yellow = moderate inhibition; green = weak/no inhibition. (B) Correlation *R* values for cell growth inhibition pIC_{50} (= $-\log_{10}$ IC_{50}, μM) or pMIC = ($-\log_{10}$ MIC, μM) between all systems investigated.

Possible Protein Targets for SQ109 and Its Analogues. The general patterns of activity seen with the compounds described above have some similarities across the diverse organisms investigated in that at least one cationic center, or perhaps more importantly a protonatable nitrogen, is required for activity. In *M. tuberculosis*, **1** is thought to act by inhibiting MmpL3, a TMM transporter,[12] although as noted by Tahlan et al., other targets could also be involved. This seems quite likely because in most cases these other organisms lack *mmpL3* or a clearly identifiable orthologue, and do not utilize TMM, as is also the case with *H. pylori*.[14] Given that protonated geranylamines might be good isosteres for transition states or reactive intermediates in enzymes involved in isoprenoid biosynthesis (Scheme 1), we investigated if **1** could inhibit any of the following enzymes: *M. tuberculosis cis*-farnesyl diphosphate synthase (Rv1086); *M. tuberculosis cis*-decaprenyl diphosphate synthase (Rv2361); *P. vivax* geranylgeranyl diphosphate synthase (GGPPS); *S. aureus* and *E. coli* undecaprenyl diphosphate synthases (UPPSs), *S. aureus* farnesyl diphosphate synthase (FPPS), and human GGPPS. In essentially all cases, IC_{50} values were $\geq$50 μM. The exception was human GGPPS, which was inhibited by **1** (the only compound with two basic groups) with a 4.5 μM IC_{50}. These enzymes are all so-called *cis* or *trans*-"head-to-tail" prenyl-transferases[18] and the presence of the two (as opposed to one) hydrophobic domains (in addition to the cationic center) might not be required for enzyme inhibition. There are, however, other prenyl transferases that might be targeted in which two hydrophobic domains, together with a carbocation center, would better mimic transition states/reactive intermediates. These would include the so-called "head-to-head" prenyl transferases, as well as some of the enzymes involved in quinone biosynthesis. There are demonstrated or putative head-to-head prenyl transferases in *M. tuberculosis* (Rv3397c), *M. smegmatis*, (Mycsm_04912), *S. aureus* (CrtM), *B. subtilis* (YisP), *S. cerevisiae* (squalene synthase, SQS), and *C. albicans* (SQS) and in humans (SQS), but no homologous proteins can be found by standard BLAST searches in *P. falciparum*. The products (where known) of these enzymes vary, and not all are essential for survival in vitro. Nevertheless, we tested a subset of compounds (**1**, **3**, **4**) for activity against either SaCrtM or human SQS, finding only weak activity (~100 μM) in all cases. These results support the notion that the head-to-head prenyl transferases are unlikely cell growth inhibition targets of our compounds in these organisms.

The other obvious candidates are the enzymes involved in quinone biosynthesis (Scheme 2) or quinone utilization. We thus next investigated the two quinone biosynthesis enzymes, MenA and MenG, both of which are likely to utilize cationic transition states/reactive intermediates during catalysis. MenA (EC 2.5.1.74, 1,4-dihydroxy-2-naphthoate polyprenyl transferase) catalyzes the isoprenylation of 1,4-dihydroxy-2-naphthoic acid by long chain isoprenoid diphosphates,[19] Scheme 2, and MenA is of interest as an *M. tuberculosis* drug target.[20−22] In an initial set of experiments we tested three potent *M. tuberculosis* and *M. smegmatis* growth inhibitors (**1**, **3**, and **13**) in the *M. smegmatis* MenA (MsMenA) membrane fragment inhibition assay described previously,[20−22] finding IC_{50} values of ~6 μM (Table 2). Typical dose−response curves are shown in Figure S1A, Supporting Information. While this assay revealed only modest activity, the observation that MenA activity was in fact inhibited by the three most potent inhibitors is a potentially important one because this inhibition might be expected to inhibit electron transfer/ATP synthesis, of particular importance in nonreplicating/persister cells,[22] and to contribute to cell growth inhibition beyond that seen with MmpL3 inhibition alone. What was also of interest was that **1** had similar activity (IC_{50} = 9 μM, in the same assay as used here[22]) against MenA to that we reported previously with Ro 48-8071, a lipophilic amine that decreases menaquinone biosynthesis and blocks *M. tuberculosis* as well as *M. smegmatis* cell growth. These growth inhibition effects with Ro 48-8071 (as well as the inhibition of respiration) were reported previously to be reversed in both organisms by addition of 400 μM menaquinone-4 (MK-4) or phylloquinone to the medium.[22]

A second possible target is MenG (EC 2.1.1.163, 2-polyprenyl-1,4-naphthoquinone methyltransferase) which carries out the *S*-adenosylmethionine (SAM)-dependent methylation of demethylmenaquinone (the product of the MenA

dx.doi.org/10.1021/jm500131s | J. Med. Chem. 2014, 57, 3126−3139

Scheme 1. Several Reactions of Interest in Isoprenoid Biosynthesis in the Systems Investigated in This Study[a]

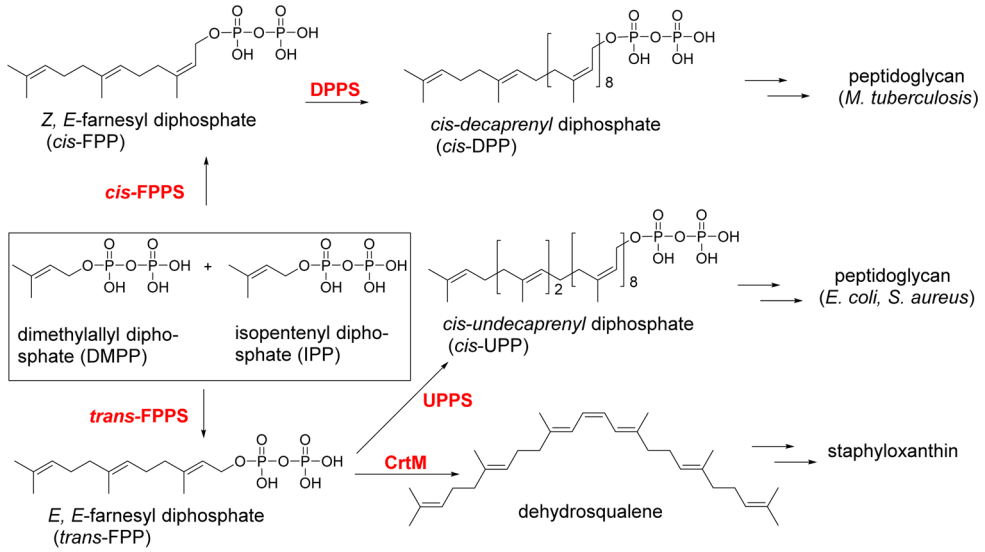

[a]The enzymes in red were tested for inhibition by **1**. *cis*-FPPS and *trans*-FPPS, UPPS, and DPPS are not inhibited by **1** but CrtM is, and CrtM-**1** structures have been reported (PDB ID 4EA1, 4EA2) and serve as models for MenA inhibition.

Scheme 2. Menaquinone Biosynthesis of MK-3[a]

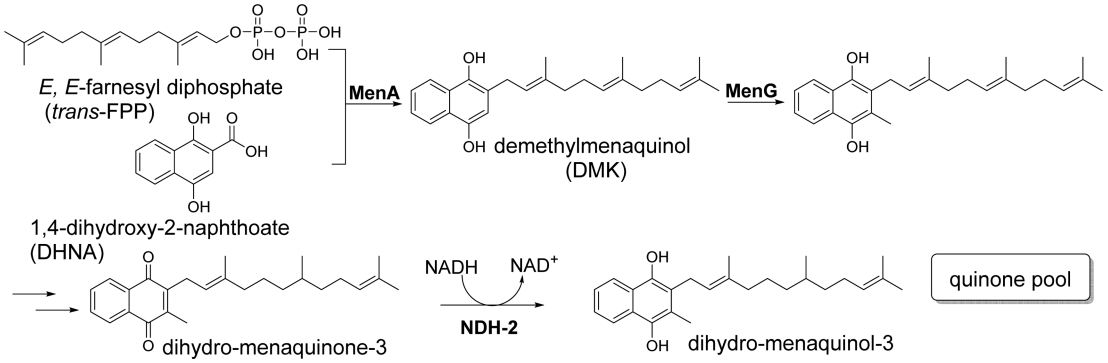

[a]MK-8,9 are the abundant species in cells. MenA forms demethylmenaquinol (DMK), which spontaneously oxidizes to demethylmenaquinone. DMK is the substrate of MenG.

reaction). As with MenA, the MenG reaction is inhibited by **1** and the potent ethanolamine analogues **3**, **13** (Table 2, and Figure S1B,C, Supporting Information), with IC_{50} in the 6−13 μM range. Unlike the C-alkylations with prenyl diphosphates, the MenG reaction uses SAM (as a C_1 source), and Mg^{2+} is not required. With **1** binding to MenG, the cationic center in the inhibitor might mimic a cationic transition state/reactive intermediate, although another possibility is that the cationic center simply mimics the SAM *S*-methyl sulfonium group. Thus, both MenA and MenG are inhibited in vitro by **1** and its analogues, which can be expected to supplement MmpL3-based inhibition in the mycobacteria, as well as provide alternative targets in some of the organisms that lack the *mmpL3* gene. Moreover, inhibition of two sequential targets (series inhibition) in a biosynthetic pathway can often be quite effective because the product of the first reaction is the substrate for the second reaction.[23]

We next used an expressed *E. coli* MenA (hereafter EcMenA) detergent-based assay to obtain inhibition data for all 12 inhibitors, Table 2, and Figure S2, Supporting Information. Interestingly, the most potent inhibitor was **3** (IC_{50} = 400 nM), and **3** was also the most potent inhibitor of *M. tuberculosis* cell growth (and, within experimental error, of *E. coli* cell growth, Table 1). We additionally found that there was a moderate correlation between *E. coli* cell growth inhibition and EcMenA inhibition with an R^2 = 0.43 (using $pIC_{50} = -\log_{10} IC_{50}$, both values in μM) values, suggesting that MenA inhibition may be involved in cell growth inhibition. As described below, the experimental vs predicted *E. coli* cell growth inhibition correlation increased to R^2 = 0.77 with the incorporation of a second experimental parameter, ΔpH collapse.

The structure of MenA is not known, but it is predicted to be a transmembrane protein containing about nine α-helices, as shown in Figure 3A.[24] Using modern structure prediction programs such as Phyre2[25] that are secondary-structure based, MenA is predicted (Figure 3B) to adopt basically all the same α-helical folds as found in farnesyl diphosphate synthase and CrtM (the *S. aureus* dehydrosqualene synthase) but where one N- and two C-terminal helices (transmembrane helices 1, 8, and 9 in Figure 3A) are not modeled, Figure 3B. A total of 198 residues (68%) are, however, modeled at a predicted >90% accuracy, and the predicted structure has the closest similarity to the crystal structure of farnesyl diphosphate synthase from *Methylococcus capsulatus* (PDB ID 3TS7), although remarkably

dx.doi.org/10.1021/jm500131s | J. Med. Chem. 2014, 57, 3126−3139

Table 2. Enzyme, Respiration, and PMF (ΔpH, Δψ) Inhibition Results

	Mycobacterium smegmatis				*Escherichia coli*	
entry	MenA[a]	MenG[a]	respiration[b]	Δψ collapse[c]	MenA[d]	ΔpH collapse[e]
1	4.8	13	58	55	3.3	0.8
3	4	15	0.5	31	0.4	0.8
4	N.D.	N.D.	36	78	1.8	1.0
5	N.D.	N.D.	600	150	4.2	15
6	N.D.	N.D.	4.8	50	1.9	1.1
7	N.D.	N.D.	0.5	51	1.0	18
8	N.D.	N.D.	330	150	5.8	12
9	N.D.	N.D.	280	150	16	7.4
10	N.D.	N.D.	9500.0	150	4.6	4.7
11	N.D.	N.D.	2500.0	150	4.6	6.7
12	N.D.	N.D.	140.0	130	3.3	7.1
13	8	5.7	0.3	44	3.2	0.8

[a]IC_{50} in μM, *M. smegmatis* membrane fraction (Figure S1, Supporting Information). [b]IC_{50} in μM, from methylene blue reduction assay (Figure S3, Supporting Information). [c]IC_{50} in μM, from DisC3(5) assay (Figure S7, Supporting Information). [d]IC_{50} in μM, expressed *E. coli* MenA (Figure S2, Supporting Information). [e]. IC_{50} in μM, measured with *E. coli* IMVs (Figures S4 and S5, Supporting Information). N.D.: not determined

there is only a 10% residue identity. The first and second aspartate-rich motifs essential for Mg^{2+} binding and catalysis in FPPS and CrtM are located in very similar regions in the MtMenA model, as shown in the superposition with CrtM in Figure 3C (orange spheres = conserved Asps in EcMenA model; blue spheres = Asp-rich motif in CrtM). This then suggests, based on the **1**–CrtM X-ray structure,[26] the binding sites for **1** (pink) shown in Figure 3C. The two Asp-rich domains in MenA are also highly conserved, as shown by a SCORECONS[27] analysis (Table S1, Supporting Information). Although only a computational prediction, it is of interest that the highest scoring Phyre2 prediction is found with a prenyl transferase enzyme that is known to utilize a carbocation mechanism, consistent with the experimental observation that only cationic species inhibit MenA.

Menaquinone Rescue Experiments. We next measured the activity of **1** against both actively growing (*M. tuberculosis* H37Rv) and nonreplicating (streptomycin-starved *M. tuberculosis* 18b)[28] mycobacteria, using a resazurin microplate reduction assay (REMA; Figure 4). **1** had a MIC of 0.15 μg/mL against actively replicating H37Rv in this assay, as expected. It also displayed activity against the nonreplicating streptomycin-starved 18b strain (where MmpL3/TMM transport is presumably not involved because there is no cell growth), and the effects of **1** on both strains were affected by MK-4 addition (Figure 4). In the H37Rv aerobic assay, the MIC shifted from 0.15 μg/mL in the absence of MK-4 (Figure 4A) to ∼1 μg/mL when the medium was supplemented with 1 mM menaquinone, consistent with a role for **1** in inhibiting quinone biosynthesis and/or electron transport. As noted above, a remarkably similar effect was seen previously with Ro 48-8071, another lipophilic amine, at 400 μM MK-4,[22] for both *M. tuberculosis* and *M. smegmatis*. The effect of **1** against nonreplicating (streptomycin-starved 18b) bacteria, as seen by REMA as a decrease in fluorescence (lack of resazurin reduction to the highly fluorescent red resorufin) above a **1** concentration of 1 μg/mL was also blocked by MK-4 addition (Figure 4B). The activity of **1** against nonreplicating (streptomycin-starved 18b) cells was confirmed by plating and counting CFU after 7 days of drug exposure (Figure 4C) with normal 7H9 medium or with 7H9 medium containing 1 mM MK-4. As can be seen in Figure 4C, **1** at 1 μg/mL had essentially no effect on (nonreplicating) bacterial activity in the presence of MK-4 and only a small effect in the absence of MK-4. However, at 10 μg/mL **1**, while there was again a small effect on activity in the presence of MK-4, cell activity in the absence of MK-4 was reduced by ∼4 log units, consistent with a role for **1** in blocking respiration and hence ATP synthesis.

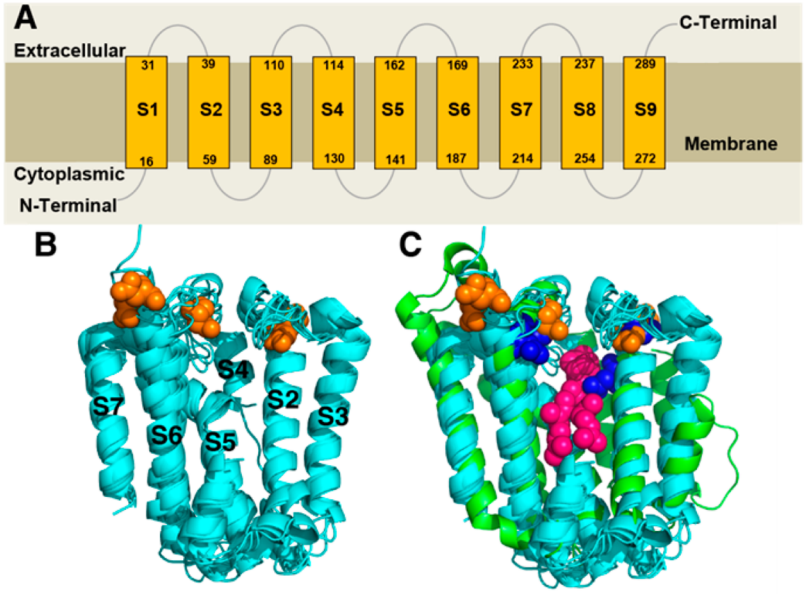

Figure 3. (A) Transmembrane helices predictions for MtMenA. (B) Transmembrane helices in Phyre2 model of MtMenA (helices S1, S8, and S9 from A are not modeled). Orange: Asp-rich motifs. (C) MenA model (cyan) and CrtM (green, PDB: 4EA1, N- and C-terminal helices are removed). Blue: Asp-rich motifs in CrtM. CrtM structure contains SQ109 (two conformers), shown as magenta spheres.

dx.doi.org/10.1021/jm500131s | J. Med. Chem. 2014, 57, 3126−3139

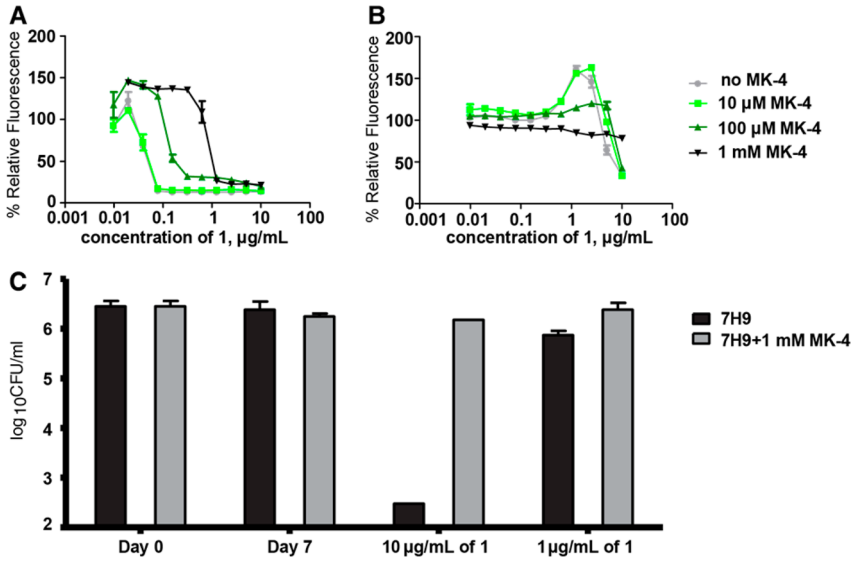

Figure 4. Menaquinone rescue experiments. (A) Aerobic *M. tuberculosis* H37Rv growth inhibition in the presence of increasing MK-4 concentrations, measured by REMA. (B) As in A but with nonreplicating *M. tuberculosis* 18b. (C) *M. tuberculosis* 18b cells were plated after 7 days of drug exposure with (gray) or without (black) MK-4. Colony forming unit counts were assessed after one month of incubation. Concentrations are in μg/mL.

Respiration, TMM, and the PMF. The results described above show that **1** has activity against not only the two mycobacteria (*M. tuberculosis* and *M. smegmatis*) but also a range of other bacteria, fungi, and a protozoan, each of which lack a bioinformatically recognizable *mmpL3* gene. In *M. tuberculosis* and *M. smegmatis*, inhibition of MenA/MenG would inhibit respiration, resulting in a decrease in ATP biosynthesis. This could help explain how **1** increases the level of TMM given that MmpL3 is a TMM transporter of the RND family of efflux pumps, many of which are powered by the PMF. Restated, **1** might exhibit an indirect action upon the TMM transporter by removing its "power source" (the proton motive force), in addition to directly binding to, and inhibiting, the transporter. This indirect action could be accomplished in one of two ways: (1) blocking respiration (by depletion of menaquinone by inhibition of MenA or MenG or by directly inhibiting a component of the electron transport chain); (2) a direct effect on the PMF ($\Delta\psi$ + ΔpH, where $\Delta\psi$ is the membrane potential and ΔpH, the pH gradient). The possibility of the involvement of the PMF is suggested from the results of a number of studies in which lipophilic bases (e.g., amiodarone, local anesthetics, and NSAIDS[29−31]) can act as uncouplers. In addition, there could also be multidrug targeting affecting MmpL3 (or efflux pumps[32]), MenA, MenG, and the PMF, which would be expected to produce potent inhibition of cell growth/respiration/ATP synthesis, as well as a low rate of resistance.

Respiration and Electron Transport. In earlier work,[21,22] we showed that several MenA inhibitors, analogues of Ro 48-8071, blocked respiration in *M. tuberculosis* and *M. smegmatis* (as evidenced by inhibiting the reduction of methylene blue), that there was a correlation between cell growth inhibition and respiration inhibition,[22] and that the effects of the inhibitors could (at least in part) be reversed by adding MK-4 at the 400 μM level. We thus next tested all compounds for their effects on methylene blue reduction, in *M. smegmatis* (Figure S3, Supporting Information), finding that there was a moderate correlation between pMIC (= $-\log_{10}$ MIC, MIC in μM) for cell growth inhibition and the pIC$_{50}$ (= $-\log_{10}$ IC$_{50}$, IC$_{50}$ in μM) for inhibition of whole cell respiration inhibition (R^2 = 0.55) for all 12 compounds (Tables 1 and 2).

These results suggest the possibility of a direct effect on electron transport (because the effects observed are rapid: tens of minutes), blocking respiration, consistent with the MK-4 rescue experiments. The nature of the target or targets involved are beyond the scope of this current study, but we did carry out preliminary experiments with **1** against a series of dehydrogenases by monitoring the reduction of the artificial electron acceptor MTT (3-(4,5-dimethyl-2-thiazolyl)-2,5-diphenyl-2*H*-tetrazolium bromide). We used an *M. smegmatis* membrane preparation and a variety of substrates including NADH (measuring both Complex I and alternative NADH dehydrogenases, NDH-2), deamino-NADH (measuring Complex I activity but not NDH-2), succinate (measuring succinate dehydrogenase), malate (measuring quinone-dependent malate dehydrogenase), and lactate (measuring lactate dehydrogenase). IC$_{50}$ values for **1** were in general ~30 μg/mL, the exception being malate dehydrogenase (IC$_{50}$ = 10 μg/mL), results that suggest that more than one-electron-transfer protein may be involved, in cells, with the inhibitors mimicking quinone substrates.

Uncoupler Effects in Membrane Vesicles and in Cells. The results presented above show that **1** and its analogues inhibit MenA, MenG, electron transfer proteins, and respiration and that MK-4 can rescue cell growth or activity, the relatively high IC$_{50}$s for enzyme inhibition/respiration (when compared to cell growth inhibition) being suggestive of multiple targeting. What is of particular interest about all of the results described above is that they seem to point in one direction: respiration, offering a possible explanation for the previous observation that TMM accumulates (with **1**), in *M. tuberculosis*, due to MmpL3 inhibition. This MmpL3 inhibition could be due to direct binding or a more indirect effect on the PMF/ATP synthesis.

To test the hypothesis that **1** and its analogues might collapse the PMF, we first used *E. coli* inverted membrane vesicles (IMVs), essentially as described by Haagsma.[33] The results

dx.doi.org/10.1021/jm500131s | *J. Med. Chem.* 2014, 57, 3126−3139

obtained with SF6847, one of the most potent uncouplers known, are shown in Figure 5A and indicate a very rapid

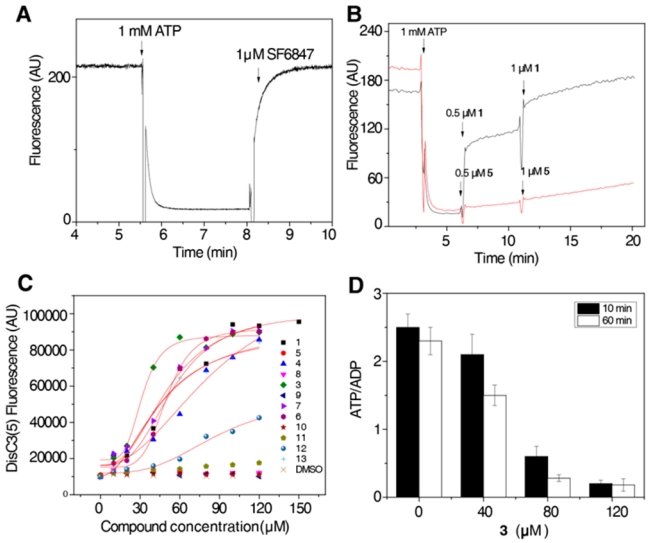

Figure 5. (A) ΔpH collapse in *E. coli* IMVs by a known uncoupler SF6847. (B) ΔpH collapse in *E. coli* IMVs by **1** and **5**. (C) Effects of **1** and analogues on Δψ in *M. smegmatis* cells. (D) Effects of **3** on ATP biosynthesis of effect in *M. smegmatis* cells.

(seconds) collapse in ΔpH, as reported by Haagsma et al.[33] The same effect was seen with **1** and analogues that have potent activity in cell growth inhibition, while inactive (diether/amide) analogues (e.g., **5**) had no effect, Figure 5B, Figures S4 and S5, Supporting Information. Similar results were obtained with both *E. coli* and *M. smegmatis* vesicles. The effects on the collapse in ΔpH were seen in vesicles in which the pH gradient was driven by either ATP hydrolysis or by electron transport in the presence of succinate or NADH. Using Oxonol VI as a probe, we also found that Δψ in *E. coli* IMVs (positive inside) was collapsed (Figure S6A) by the same compounds, and there was a correlation between the collapse of the membrane potential and the collapse in ΔpH (using ACMA fluorescence; Table 2; R^2 = 0.79, Figure S6B, Supporting Information). This is consistent with these lipophilic cations acting as protonophores, carrying protons across the membrane lipid bilayer, with only compounds containing a basic nitrogen supporting the uncoupling activity.

We found similar PMF effects in intact *M. smegmatis* cells in which there was a collapse in Δψ (positive outside), as measured by using DisC3(5) fluorescence, Figure S7, Supporting Information. Addition of **1** or the potent analogues to *M. smegmatis* cells resulted in an immediate increase in DisC3(5) fluorescence, indicating a collapse of Δψ. As can be seen in Figure S7B, Supporting Information, **1** collapses the membrane potential in a dose-dependent manner with an "EC_{50}" of ∼20 μg/mL. The EC_{50} for one of the most potent cell growth inhibitors **13** was ∼15 μg/mL.

In addition to these investigations of Δψ collapse in intact cells, we investigated ΔpH collapse in intact *M. smegmatis* cells, using ^{31}P NMR spectroscopy. Phosphorus NMR chemical shifts are sensitive indicators of local pH values.[34] As can be seen in Figure S8A, Supporting Information, the ^{31}P NMR chemical shift of phosphate inside *M. smegmatis* is ∼0.35 ppm downfield from external P_i, and from these chemical shifts, the internal and external pH values can be determined: results are shown in Figure S8B, Supporting Information. There is a ΔpH = 0.26 (inside more basic) in wild type *M. smegmatis* cells, but this pH gradient is collapsed by the uncoupler CCCP (*m*-chlorophenylcarbonyl cyanide phenylhydrazone), by the antiporter nigericin, and by **1** and **13**, while as expected, the K^+ ionophore valinomycin has no effect. The effects of **1** and the other potent analogue thus leads to collapse of Δψ as well as ΔpH in both inverted vesicles and in whole cells. This collapse in the PMF, in cells, can be expected to result in an inhibition of ATP synthesis, as is indeed found experimentally (Figure 5D) with the potent lead, **3**. In addition, the collapse of the proton motive force is expected to inhibit activity of the MmpL3/TMM transporter.

Quantitative Models for Cell Growth Inhibition. Any quantitative analysis of cell growth inhibition based on enzyme inhibition or another property (e.g., ΔpH collapse) is of course challenging, but it should be possible to use the multidescriptor approach described previously[35] with, in this case, no purely mathematical descriptors being required. We thus use eq 1:

$$pIC_{50}(\text{cell}) = a \times pIC_{50}(A) + b \times pIC_{50}(B) + c \qquad (1)$$

where $pIC_{50}(A)$ is $-\log_{10}$ (IC_{50}, A) for enzyme or property A (such as MenA inhibition), and B is a second property, e.g., ΔpH collapse. We show by way of examples in Figures 6A,B, three-dimensional plots for *E. coli* cell growth inhibition: log IC_{50} = *f* (MenA, ΔpH), and for *M. smegmatis*: log MIC = *f* (respiration, Δψ), where we find correlation coefficients of R^2 =

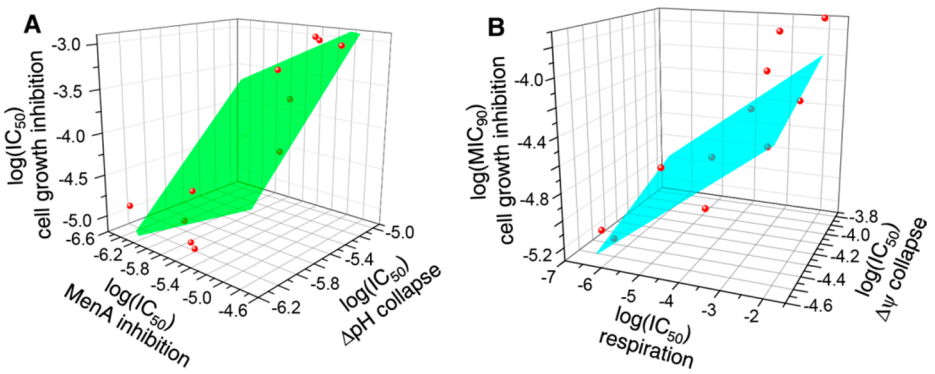

Figure 6. Experimental (red circles) and computed (colored plane) results for cell growth inhibition based on eq 1. (A) *E. coli* cell growth inhibition predicted using MenA, ΔpH collapse (IC_{50}s in μM, R^2 for the model = 0.77). (B) *M. smegmatis* growth inhibition using respiration (methylene blue assay) and Δψ collapse (MIC and IC_{50}s in μM, R^2 for the model = 0.64).

dx.doi.org/10.1021/jm500131s | J. Med. Chem. 2014, 57, 3126−3139

0.82 (*E. coli*) and R^2 = 0.72 (*M. smegmatis*) values for the experimental-versus-predicted cell growth inhibition results. In previous work we investigated correlations between cell and enzyme activity (pIC_{50}) assays in 10 diverse systems finding[35] on average an R^2 = 0.32 for the 10 cell/enzyme correlations, similar to the R^2 = 0.43 we find for the MenA alone/*E. coli* cell growth inhibition correlation. Incorporation of the second parameter (the percentage of ΔpH collapse) increases the R^2 to 0.77, suggesting the importance of multitargeting, in *E. coli*. The correlation is worse for *M. smegmatis* due, perhaps, to the omission of an MmpL3 term, expected to be particularly important in the mycobacteria.

Are There Other MenA-like Targets? The results presented above show that *E. coli* MenA is inhibited by **1** and its analogues and that there is a correlation between MenA inhibition and cell growth inhibition (in *M. smegmatis*), suggesting that diverse MenAs may be inhibited by these compounds. However, this result is perhaps surprising in that in *E. coli*, MenA is not an essential gene for aerobic growth because UbiA can be used in aerobic respiration. One possibility is that EcUbiA might also be inhibited by **1** (and its analogues). While we have not yet investigated this experimentally, what we have found is that MtMenA, EcMenA, and EcUbiA are all predicted (using the Phyre2 program) to have an FPPS/GGPPS-like structure.

In all three cases the structures are predicted to contain a central FPPS/GPPS-like catalytic domain (comprising ~2/3 of the overall amino acid sequence) that has close similarity to the same two (soluble) prenyl synthases: *Methylococcus capulatus* FPPS and *Lactobacillus brevis* GGPPS. Predicted sequence identity investigations have shown that MenA and UbiA have moderate homology,[36,37] but correlations with FPPS and GGPPS were not made in those studies because the actual sequence identities are very low, about 10−16%. However, secondary-structure-based algorithms do permit accurate structure predictions, even when residue identities are low.

These previous bioinformatics studies also demonstrated that another class of proteins, protoporphyrin IX farnesyl transferases (e.g., heme o synthase), have significant sequence homology to the MenA/UbiA proteins, and all three classes of proteins are Mg^{2+}-dependent prenyl transferases. Once again, the structure of heme o synthase is not known but is predicted to be another nine-helix transmembrane protein with a central FPPS/GGPPS-like core, suggesting that MenA, UbiA, and protoporphyrin IX farnesyl transferases are all likely to be inhibited by **1** and related systems.

MmpL3 and MmpL11 as Targets. MmpL3 is thought to be a target for **1** (and other diverse inhibitors[12,13,38,39]), blocking TMM transport. It has also been shown that MmpL3 together with a related protein, MmpL11, is associated with heme uptake.[40,41] The X-ray structures of MmpL3 and MmpL11 have not been reported. However, both are membrane proteins and are predicted to have 11−12 transmembrane helices.[24] Using the Phyre2 program,[25] we find with MmpL3 that 653 residues (69% coverage) are predicted with 100% confidence to have the structure shown in Figure 7A and with MmpL11, 642 residues (66% coverage) are predicted with 100% confidence to have the structure shown in Figure 7B. Both structures are very similar to those found in cation efflux pumps such as CusA (PDB ID 3ko7) and multidrug efflux pumps such as the acriflavin resistance protein B (AcrB; PDB ID 1oy8), although the C-terminus (~1/3 of the total protein) is not modeled in either MmpL3 or MmpL11.

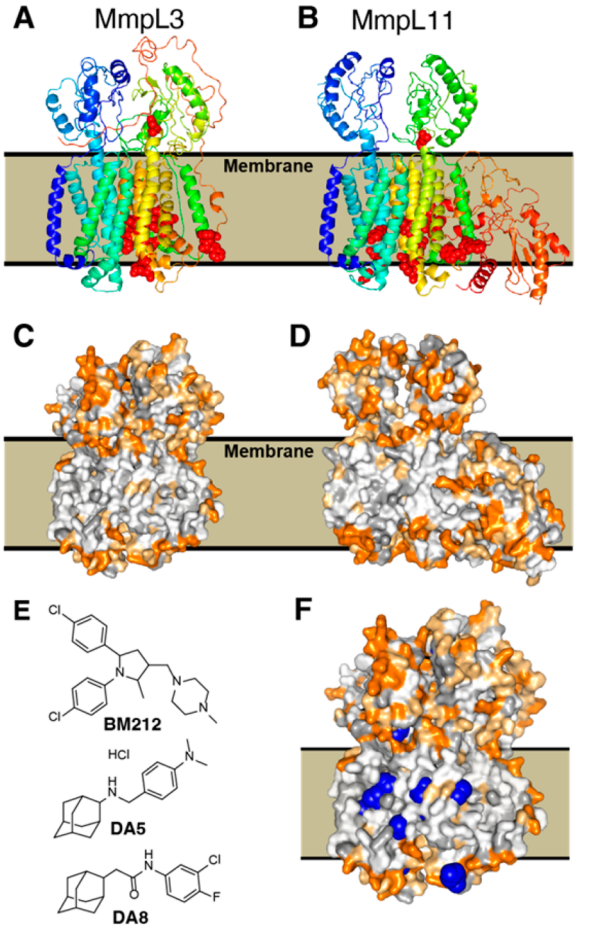

Figure 7. Molecular models for MmpL3, MmpL11. (A) Phyre2 structure predictions for MmpL3. (B) Phyre2 structure predictions for MmpL11. (C) Phyre2 predictions showing hydrophobic residues (white/gray) and their proposed relation to the membrane for MmpL3. (D) Phyre2 predictions showing hydrophobic residues (white/gray) and their proposed relation to the membrane for MmpL11. (E) Structure of representative *M. tuberculosis* growth inhibitors that are thought to target MmpL3 and (F) sites of resistance mutations (blue spheres) in MmpL3.

The transmembrane hydrophobic domains are shown in Figure 7C,D (in white/light orange). **1** as well as several other inhibitors[12,13] (Figure 7E) has been proposed to target MmpL3 (detected by sequencing mutants that arose under drug pressure), but the sites of these mutations, shown as blue spheres in Figure 7F, are spread throughout the protein, suggesting, perhaps, multisite targeting of MmpL3/11 as an additional basis for the lack of resistant mutations with **1**. Overall, however, the effects of **1** on the PMF and respiration, the menaquinone-reversal experiments, activity against diverse organisms as well as the ability to make generally good predictions of cell activity without MmpL3 inhibition data suggests that MmpL3 may not be the primary target for **1**, in *M. tuberculosis*. In addition, of course, other targets may exist.

A Multitarget Model for Antiinfective Activity. We show in Figure 8 a summary of the proposed sites of action for **1** and its analogues in *M. tuberculosis* and in *M. smegmatis*. Some of these targets are also present in the other pathogens investigated but not in human cells. In addition to its previously proposed role in targeting MmpL3, **1** and its analogues also inhibit MenA and MenG and, as described above, the inhibition

dx.doi.org/10.1021/jm500131s | J. Med. Chem. 2014, 57, 3126−3139

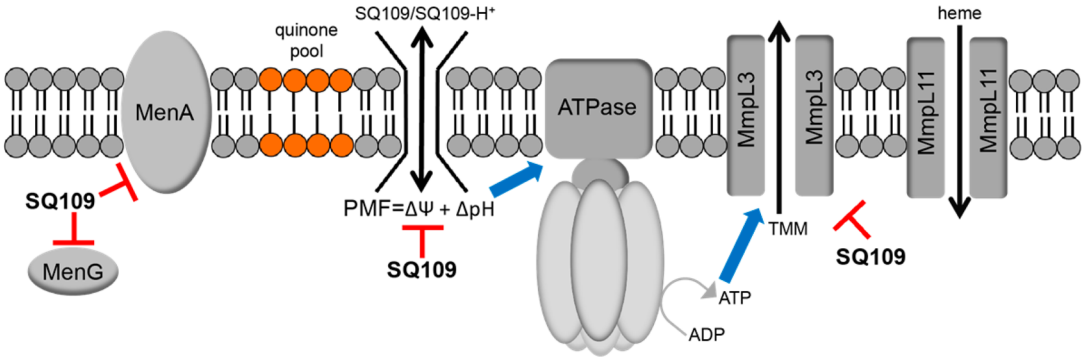

Figure 8. Proposed sites of action of SQ109 and its analogues. MenA, MenG targeting can affect respiration/electron transfer; PMF (ΔpH, Δψ) collapse leads to decreased ATP biosynthesis, reduction in PMF/ATP-powered transporters (e.g., MmpL3), increased TMM accumulation, and decreased cell wall biosynthesis.

of *M. tuberculosis* cell growth or activity is rescued by MK-4. We also find that the PMF is inhibited by the most active compounds, which act as protonophores/uncouplers. This results in a decrease in ATP synthesis and, we propose, decreased activity of MmpL3/11, helping explain the accumulation[12] of TMM (with **1**).

This multiple-targeting is perhaps best thought of as involving network inhibition in which both series and parallel paths are involved (Figure 1C) because at least in the mycobacteria, MenA, MenG, electron transport, ΔpH, Δψ, and MmpL3 (and presumably other pumps dependent on the PMF) can all be affected. There are, of course, likely to be differences in the mechanisms of action of different inhibitors in different organisms (and in the same organisms under different growth conditions), although effects on the PMF are expected to be quite common because they are based on more "physical" properties, rather than purely enzyme inhibition. The uncoupling effects we observe could also help explain the growth inhibition seen in human cell lines, as could inhibition of the human MenA, UbiA, and MenG/UbiE orthologues: UbiAD1, CoQ2, and CoQ3.

Also of interest are the likely differences in time scales (and concentrations) for the different reactions involved. The effects on the collapse in Δψ and ΔpH are very rapid-on the seconds to minutes time scale and are observed (in vesicle experiments) at low μM concentrations, for the most active species. The effects on respiration as determined by methylene blue reduction (in intact cells) are also rapid, typically observable in minutes, and may reflect the time required for inhibitors to enter the cell and accumulate (because they could also be actively pumped out). Little is known about the rate of menaquinone turnover, but it is likely that several cell divisions are required for a large reduction in menaquinone levels, so while MenA/MenG inhibition may be rapid, the effects on cell growth may take many hours or (with *M. tuberculosis*) days to occur likewise, because MmpL3 is thought to be involved in cell wall biosynthesis, its inhibition would also be expected to result in observable effects on growth inhibition on a time scale of hours to days.

CONCLUSIONS

The results we have described above are of interest for drug discovery against tuberculosis, as well as against other bacterial, fungal, and protozoan pathogens, for several reasons. We synthesized a series of analogues of the antituberculosis drug **1** in which we varied the nature of the ethylenediamine linker to provide cationic, protonatable, and neutral species, and in addition we varied the adamantyl headgroup. The most active compound against *M. tuberculosis* was ∼5× more potent than was **1** and was also less toxic to an MCF-7 human cell line. We tested all compounds against a panel of bacteria, fungi, and a protozoan parasite, and the results obtained showed that at least one cationic (or basic) group was essential for activity. The most potent activity was against *M. tuberculosis* (MIC = 0.02−0.05 μg/mL) and the intraerythrocytic form of the malaria parasite, *P. falciparum* (IC_{50} = 30 ng/mL). To explore possible targets, we tested several compounds for activity against a panel of *cis*- and *trans*-prenyl transferases (*cis*-FPPS, FPPS, DPPS, GGPPS, UPPS, CrtM, and SQS) as well as against the menaquinone biosynthesis enzymes, MenA and MenG. Activity was seen against MenA and MenG, and we proposed a structural model for the MenA active site, as well as a likely binding site for **1**. In addition, we found that menaquinone (MK-4) rescued both aerobic H37Rv *M. tuberculosis* cell growth and the activity of nonreplicating *M. tuberculosis* (streptomycin-starved 18b). We found that **1** as well as several analogues inhibited oxygen consumption in *M. smegmatis*, and there was a correlation between oxygen consumption and cell growth inhibition. We tested **1** and each of the 11 analogues for their effects on the PMF (ΔpH and Δψ) in fluorescence-based assays, as well as in some cases in intact cells (via ^{31}P NMR). The results obtained showed that **1** and the most potent cell growth inhibitors collapsed both Δψ and ΔpH, and there were good correlations between experimental and predicted cell growth inhibition results based on MenA/ΔpH (*E.coli*) and respiration/Δψ (*M. smegmatis*). Taken together, the results obtained suggested a model for **1**/analogue activity in mycobacteria in which the increase in TMM levels seen on treatment with **1** have a contribution from (indirectly) inhibiting the TMM transporter MmpL3 by blocking the PMF/ATP biosynthesis. Overall, the results are of general interest because they indicate that **1** (and its analogues) can have diverse effects: on O_2-consumption/electron transport/MenA/MenG inhibition; on Δψ, ΔpH, and ATP biosynthesis, likely helping to explain activity against non-MmpL3-containing pathogens such as *H. pylori*, *C. albicans*, and, here, *P. falciparum*. Moreover, the possibility of developing more potent compounds that can inhibit these targets is of general interest in the context of developing drug leads that are "resistance resistant", due to multitargeting.

dx.doi.org/10.1021/jm500131s | J. Med. Chem. 2014, 57, 3126−3139

EXPERIMENTAL SECTION

Chemical Syntheses: General Methods. All chemicals were reagent grade and were used as received. Moisture-sensitive reactions were performed under an inert atmosphere (dry nitrogen) with dried solvents. Reactions were monitored by TLC using Merck silica gel 60 F-254 thin-layer plates. Flash column chromatography was carried out on Merck silica gel 60 (230−400 mesh). ^{1}H NMR and ^{13}C NMR spectra were recorded on Varian (Palo Alto, CA) Unity spectrometers at 400 and 500 MHz for ^{1}H and at 100 and 125 MHz for ^{13}C. Coupling constants (J) are reported in hertz. High-resolution mass spectra (HRMS) were recorded in the University of Illinois Mass Spectrometry Laboratory. Elemental analyses were carried out in the University of Illinois Microanalysis Laboratory. HPLC/MS was performed using an Agilent LC/MSD Trap XCT Plus system (Agilent Technologies, Santa Clara, CA) with an 1100 series HPLC system including a degasser, an autosampler, a binary pump, and a multiple-wavelength detector. All final compounds were ≥95% pure as determined by elemental analysis, analytical HPLC/MS analysis, or qNMR analysis. qNMR spectra were recorded using Varian (Palo Alto, CA) 500 MHz Unity spectrometers with 1,3,5-trimethoxybenzene as the internal total-spin-count quantitation standard; 60° pulse excitation, 60 s recycle delay, 1.0 Hz line-broadening due to exponential multiplication, and 16 accumulations. qNMR data were processed using Mnova NMR software (Mestrelab, Escondido, CA). All NMR spectra (including qNMR spectra) are provided in the Supporting Information.

Enzyme Inhibition Assays. *MenA and MenG Inhibition.* MenA and MenG inhibition assays were carried out using *M. smegmatis* membrane fragments.[22] Mycobacterial MenA assays were conducted as previously reported.[22] In addition, we used an expressed, purified *E. coli* MenA, as described below.

MenG Assay. Vitamins K1 and K2 and kanamycin were purchased from Sigma-Aldrich (St. Louis, MO). Authentic MK9 was purchased from Toronto Research Chemicals (TRC, Canada). *S*-Adenosyl-L-[methyl-^{14}C]methionine (^{14}C-SAM) obtained from Perkin-Elmer (47 mCi/mmol). DMK8 was prepared from an *E. coli* Δ*ubiE* mutant (CGSC #11636), which accumulates DMK8, and was purchased from the *E.coli* Genetic Stock Center, Yale University (http://cgsc.biology.yale.edu).

MenG assays were conducted using the membrane fractions prepared from *M. smegmatis* grown in 7H9 medium (supplemented with oleic acid, albumin, dextrose, and 0.05% Tween 80). Washed cells were resuspended in buffer A (50 mM MOPS pH 7.9, 5 mM $MgCl_2$, 5 mM DL-dithiothreitol (DTT), 10% glycerol (V/V)) and disrupted by probe sonication on ice with a Sanyo Soniprep 150 (10 cycles of 60 s on and 90 s off). The whole cell lysate was centrifuged at 27 000*g* for 20 min at 4 °C. The supernatant was further centrifuged at 100 000*g* (for 2 h at 4 °C) in an Optima TLX Ultracentrifuge (Beckman). The membrane-enriched pellet was washed with buffer A followed by ultracentrifugation at 100 000 g. The washed pellet was resuspended in buffer A, divided into aliquots, and frozen at −80 °C. The membrane protein concentration was estimated by using a BCA protein assay kit (Pierce).

Assay mixtures (100 μL) contained 100 mM Tris-HCl pH 8.0, 1 mM DTT, 5 mM $MgCl_2$, 0.1% CHAPS, 600 ng of DMK8, 40 μM radiolabeled SAM, and varying concentrations of inhibitor **1** (0 to 25.0 μg/mL). Reactions were initiated by the addition of 50−100 μg of *M. smegmatis* membrane protein and incubated at 37 °C for 1 h. Reactions were stopped by the addition of 0.1 M acetic acid in methanol (0.5 mL), and radiolabeled products were extracted with hexane (2 × 3 mL). Pooled extracts were washed with 1 mL of water, evaporated to dryness under a N_2 stream, and dissolved in $CHCl_3/CH_3OH$ (2:1 v/v). An aliquot was subjected to liquid scintillation counting (LS 6500, Beckman Coulter); a second aliquot and authentic standards (DMK8 and MK9) were subjected to reverse-phase TLC (Whatman KC 18F Silica gel 60 A) developed in acetone/water (97:3). Standards were visualized under UV light, and distribution of radioactivity was detected by phosphorimaging (Typhoon TRIO, Amersham Biosciences) and quantified with ImageQuant TL v2005 software (Amersham Biosciences). IC_{50} values were calculated by using GraFit Software (Version 5.0.13).

Expression and Purification of EcMenA. The gene encoding EcMenA with a N-terminal strep tag was amplified by polymerase chain reaction (PCR) with forward primer 5′-GACGACGACAAGATGAGCGCGTGGAGCCATCCGCAGTTTGAAAAAGGCGGTGGCAGCGCGGAGAATCTTTATTTTCAGGGCGCTGGTGC-3′ and reverse primer 5′-GAGGAGAAGCCCGGTTATTATGCTGCCCACTGGCTTAGGAATAT-3′, and then cloned into the pET46 Ek/LIC vector. The recombinant plasmid was transformed to *E. coli* C43 (DE3) and the protein induced with 1 mM isopropyl thiogalactopyranoside (IPTG) at 37 °C for 5 h. The cell paste was harvested by centrifugation at 7000*g* and resuspended in buffer A containing 25 mM Tris-HCl, pH 7.5, 150 mM NaCl, and 20 mM imidazole. A cell lysate was prepared with a JNBIO pressure cell (JN-3000 PLUS), the membrane, and soluble proteins being separated by ultracentrifugation at 150 000*g* for 1.5 h. The resulting pellet was solubilized by incubation in buffer A supplemented with 1% (w/v) DDM detergent overnight at 4 °C. The latter solution was centrifuged (100 000*g* for 1 h at 4 °C in a Beckman Ti70 rotor) and the supernatant loaded onto a Ni-NTA column and washed with buffer A containing 0.05% DDM. The buffer and gradient for the Ni-NTA column were 25 mM Tris, pH 7.5, 150 mM NaCl, 0.05% DDM, and 20−500 mM imidazole. The protein was then loaded onto a Strep-Tactin (IBA) column equilibrated with washing buffer containing 100 mM Tris-HCl, pH 8.0, 150 mM NaCl, 1 mM EDTA, and 0.05% DDM and washed with five column volumes of washing buffer. EcMenA was finally eluted with eluting buffer containing 100 mM Tris-HCl, pH 8.0, 150 mM NaCl, 1 mM EDTA, 0.05% DDM, and 2.5 mM desthiobiotin. The purified protein was finally concentrated to 5 mg mL^{-1} in a 25 mM Tris-HCl, pH 7.5, 150 mM NaCl, 0.05% DDM buffer.

EcMenA Inhibition Assay. Inhibition of EcMenA was carried out using an HPLC-based protocol. Typically, 2.5 μg of EcMenA in 100 μL of reaction buffer (25 mM Tris-HCl, 0.1% Triton X-100, 250 μM $MgCl_2$, 10 mM DTT, pH = 7.5) was incubated with inhibitors for 30 min at 22 °C. 1,4-Dihydroxy-2-naphthoic acid (DHNA) and farnesyl diphosphate (FPP) were then added to the enzyme solution to a final concentration of 150 μM each. The reaction was incubated at 37 °C for 3 h before quenching with 50 μL of 0.1 M acetic acid in methanol containing 50 μM menaquinone-4 (MK-4, Sigma-Aldrich) as an internal standard. The mixture was then extracted with 600 μL of hexane by vortexing. After centrifugation, 500 μL of organic layer was collected and dried under nitrogen then dissolved in 200 μL of methanol. Twenty microliters of the methanol solution was then subjected to HPLC analysis (0.1% formic acid in H_2O to 0.1% formic acid in CH_3CN, UV: 325 nm, 250 μL/min). The amount of the MenA reaction product demethylmenaquinone-3 (DMMK-3) was determined by comparison of integrated peak areas between DMMK and the internal standard MK-4. IC_{50} values were estimated by using Origin 6.1 software to analyze the dose−response curves.

Cell Lines. *Mycobacterium tuberculosis* ATCC 27294, *Mycobacterium smegmatis* ATCC 700084, *Bacillus subtilis* subsp. *subtilis* ATCC 6051, *E. coli* ATCC 29425, and *Saccharomyces cerevisiae* ATCC 208352 were purchased from the American Type Culture Collection. The *C. albicans* strain was CAI-4; the *P. falciparum* strain was 3D7 and the human cell line MCF-7 (breast adenocarcinoma), obtained from the National Cancer Institute.

***M. tuberculosis* Growth Inhibition Assay.** All 12 compounds (**1**, **3**−**13**) were assayed for inhibition of *M. tuberculosis* cell growth as described previously.[42]

Menaquinone Rescue Experiments with *M. tuberculosis* Treated with 1. We measured the activity of **1** against both actively growing *M. tuberculosis* (H37Rv) and nonreplicating *M. tuberculosis* (streptomycin-starved 18b[28]) using a resazurin microplate reduction assay. The effects of menaquinone supplementation on the dose−response curves were investigated using medium that was supplemented with 0, 10, 100, and 1000 μM menaquinone (MK-4, Sigma-Aldrich) in the presence of between 10 ng/mL and 10 μg/mL **1**. The activity of **1** against nonreplicating 18b was determined after 7 days of drug exposure by plating the culture followed 28 days later by

dx.doi.org/10.1021/jm500131s | J. Med. Chem. 2014, 57, 3126−3139

CFU counting after plating serial dilutions on 7H10 agar plates (Difco) .

***Candida albicans* Growth Inhibition Assay.** *C. albicans* growth inhibition was carried out according to a reported protocol[43] except that YPD media was used instead of RPMI 1640.

***E. coli* Growth Inhibition Assay.** IC_{50} values for *E. coli* growth inhibition were determined by using a broth microdilution method. An overnight culture of *E. coli* was diluted 50-fold into fresh Luria−Bertani (LB) broth and incubated to an OD_{600} of ∼0.4. The culture was then diluted 500-fold into fresh LB medium and 100 μL inoculated into each well of a 96-well flat-bottom culture plate (Corning Inc., Corning, NY). The starting concentration of each compound was 0.3 mM, and this was 2× serially diluted to 292 nM. Plates were incubated for 3 h at 37 °C to midexponential phase. An MTT ((3-(4,5-dimethylthiazol-2-yl)-2,5-diphenyltetrazolium bromide) cell proliferation assay (ATCC) was then carried out to obtain bacterial viability dose−response curves. Briefly, 10 μL of MTT reagent was added into each well, followed by incubation for 2−4 h until a purple precipitate was visible. Then, 100 μL of detergent reagent was added, and the plates were incubated in the dark at 22 °C for 2 h. Absorbance was measured at 570 nm and a nonlinear regression analysis carried out using Origin 6.1 software.

***B. subtilis* Growth Inhibition Assay.** IC_{50} values for *B. subtilis* growth inhibition were determined by using a microbroth dilution method. A stationary starter culture of *B. subtilis* was diluted 50-fold into fresh LB broth and grown to an OD_{600} of ∼0.4. The culture was then diluted 500-fold into fresh LB medium to give a working solution, and then 100 μL of working solution was transferred to each well of a 96-well flat-bottom culture plate (Corning Inc., Corning, NY). Inhibitors were then added at 0.5 mM and 2× serial diluted to 500 nM, the volume and solvent composition constant. Plates were incubated for 12−16 h at 37 °C, and the absorbance at 600 nm was determined. A nonlinear regression analysis was carried out using Origin 6.1 to obtain the IC_{50} values.

***S. cerevisiae* Growth Inhibition Assay.** The protocol was the same as for *B. subtilis* except that YPD instead of LB was used as the culture medium, and the 96-well plates were incubated for 48 h instead of 12−16 h.

***Plasmodium falciparum* Growth Inhibition Assay.** We determined IC_{50} values for *P. falciparum* growth inhibition using the intraerythrocytic assay described previously.[44]

Human Cell Growth Inhibition Assay. The MCF-7 cell growth inhibition assay was carried out as described previously.[45] A broth microdilution method was used to determine the growth inhibition IC_{50} values. Compounds were half-log serial diluted using cell culture media into 96-well TC-treated round-bottom plates (Corning Inc., Corning, NY). Cells were plated at a density of 5000 cells/well and then incubated under the same culture conditions for 2 days at which time an MTT ((3-(4,5-dimethylthiazol-2-yl)-2,5-diphenyltetrazolium bromide) cell proliferation assay (ATCC, Manassas, VA) was performed to obtain dose−response curves.

Dehydrogenase Activities. Dehydrogenase activity in *M. smegmatis* membranes was measured by using the MTT ((3-(4,5-dimethylthiazol-2-yl)-2,5-diphenyltetrazolium bromide) reduction assay in the presence of 5 mM KCN. MTT reduction was followed at 570 nm, after addition of the different substrates (NADH, succinate, malate, or lactate).

Oxygen Consumption. Oxygen concentration was monitored at 37 °C using a YSI model 53 oxygen electrode (Yellow Springs Instrument Co., Yellow Springs, OH) equipped with a temperature-controlled 1.8 mL electrode chamber. The reaction mixture consisted of sodium phosphate buffer, pH 7.5, 50 mM NaCl, and 200−400 μg/mL membranes. The concentration of oxygen in the air-saturated buffer was taken to be 250 μM, and the reaction was initiated by injecting 200 μM NADH. The electron transport rates are expressed as mol of NADH oxidized or mol of O_2 (mol enzyme)$^{-1}$ s^{-1}. Membranes were incubated with different concentrations of inhibitors for 5 min prior to NADH addition.

Membrane Potential Measurements in Intact Cells. The effects of inhibitors on Δψ were determined by fluorescence quenching of the potential-sensitive probe 3,3′-dipropylthiodicarbocyanine (DisC3(5)). *M. smegmatis* were grown for 8 h in Middlebrook 7H9-ADC-Tween 80 medium and diluted to an OD_{600} of 0.3 in the same medium plus 10 mM glucose and 1 μM nigericin. Different concentrations of **1** and its analogues were added to the bacterial suspension, and changes in fluorescence due to the disruption of Δψ were continuously monitored with a fluorescence spectrophotometer (FLUOstar Omega, BMG LABTECH) employing an excitation wavelength of 643 nm and an emission wavelength of 666 nm, at 30 °C.

ATP/ADP Determination. *M. smegmatis* were grown for 8 h in Middlebrook 7H9-ADC-Tween 80 and diluted to an OD_{600} of 2. Different concentrations of **1** and its analogues were added and ATP/ADP ratios determined (Abcam; ADP/ATP Ratio Assay Kit, catalog number: ab65313) after 10 and 60 min of incubation at 37 °C, 200 rpm. ATP and ADP were extracted from 50 μL of cell suspension by adding trichloroacetic acid (TCA) to a final concentration of 0.5%. After 5 min, TAE (Tris−acetic acid−EDTA) buffer was added to neutralize the system by diluting the sample 5-fold. The ATP and ADP cell concentrations were measured according to the manufacturer's protocol.

Inverted Membrane Vesicles (IMVs). *E. coli* IMVs were prepared by three passages through a precooled French pressure cell at 20 000 psi. The lysate was centrifuged at 14 000*g* at 4 °C for 20 min to remove unbroken cells. The supernatant was centrifuged at 370 000*g* at 4 °C for 1 h, and the pellet, consisting of the IMVs, was washed with 50 mM MOPS−KOH (pH 7.5), 2 mM $MgCl_2$. After the second centrifugation step, membranes were resuspended in 50 mM MOPS−KOH (pH 7.5), 2 mM $MgCl_2$, 10% glycerol, and stored at −80 °C.

Assay for ATP or Succinate-Driven Proton Translocation. Proton translocation into IMVs was measured by the decrease of ACMA fluorescence. The excitation and emission wavelengths were 410 and 480 nm, respectively. IMVs (0.1 mg/mL membrane protein) were preincubated at 37 °C in 10 mM HEPES−KOH (pH 7.5), 100 mM KCl, 5 mM $MgCl_2$ containing 2 μM ACMA, and the baseline was monitored for 5 min. The reaction was then initiated by adding 1 mM ATP or 5 mM succinate. When the signal had stabilized, **1** or its analogues were added and proton translocation was measured, fluorimetrically.

Determination of Δψ Collapse in IMVs. The Δψ-sensitive fluorophore Oxonol VI (1,5-bis(5-oxo-3-propylisoxazol-4-yl)-pentamethine oxonol) was used to determine if **1** and its analogues were able to dissipate the membrane potential in IMVs. IMVs (0.1 mg/mL membrane protein) were added to assay buffer: 10 mM MOPS−KOH pH 7.5, 2 mM $MgCl_2$, 2 μM Oxonol VI. After a few seconds, 0.5 mM NADH was added to initiate respiration-dependent generation of Δψ (positive inside), and the resultant quenching of Oxonol VI fluorescence was monitored at 37 °C. The emission and excitation wavelengths were 599 and 634 nm, respectively. Uncoupling by inhibitors was estimated based on their ability to dissipate the established Δψ, measured as the dequenching of the fluorescence signal.

Determination of ΔpH by ^{31}P NMR Spectroscopy. *M. smegmatis* was grown to a cell density of 10^8 cells/mL in a total volume of 500 mL in a 4 L Erlenmeyer flask with constant shaking at 37 °C in Difco Middlebrook 7H9 media supplemented with oleic acid/albumin/dextrose and 0.05% Tween 80. Cells were harvested by centrifugation, and the pellet was washed twice with 5 mM phosphate buffer, pH 6.8. The cell pellet was then resuspended in 200 μL of the same buffer and 500 μL of the resulting cell slurry transferred to a 5 mm NMR tube. Chemical shifts were referenced with respect to 85% phosphoric acid in D_2O in a coaxial capillary. ^{31}P NMR spectra were obtained using a Varian INOVA 300 (at 121.5 MHz) using 60° pulse excitation, proton decoupling, and a 1 s recycle time. A total of 1024 scans were accumulated corresponding to approximately a 60 min total data acquisition time (without aeration). Spectra were analyzed as described elsewhere.[46] The peak corresponding to the α-phosphate of ATP (at ∼−10.5 ppm) and the inorganic phosphate peaks of interest (in the region of 0−1.5 ppm) were used to calculate the internal and external pH using the following equation, where *d* is the distance

dx.doi.org/10.1021/jm500131s | J. Med. Chem. 2014, 57, 3126−3139

between the α-phosphate of ATP and the inorganic phosphate peak, in ppm.

$$\mathrm{pH} = 6.75 + \log \frac{d - 10.85}{13.25 - d}$$

■ ASSOCIATED CONTENT

Supporting Information

Additional table and figures illustrating SCORECONS analysis of MtMenA, MenA/MenG inhibition, methylene blue reduction assay, $\Delta\psi$ dissipation, NMR measurement of ΔpH, ACMA fluorescence results, synthesis schemes and protocols, compound characterization and purity data, and NMR (including qNMR) spectra. This material is available free of charge via the Internet at http://pubs.acs.org.

■ AUTHOR INFORMATION

Corresponding Author

*Tel: 217-333-3374. Fax: 217-244-3186. E-mail: eoldfiel@illinois.edu.

Author Contributions

[&]These authors contributed equally.

Notes

The authors declare no competing financial interest.

■ ACKNOWLEDGMENTS

This work was supported by the United States Public Health Service (National Institutes of Health grants GM065307, CA158191, HL016101, and AI049151), the National Basic Research Program of China (grants 2011CB710800 and 2011CBA00805), the National Research Foundation of Korea (NRF) funded by the Korean government (MSIP, no. 2007-00559), Gyeonggi-do (no. K204EA000001-09E0100- 00110), and KISTI, and by a grant from the NIH Director's New Innovator Award Program (DP2 OD008463 to D.A.M.), the European Community's Seventh Framework Programme (Grant 260872, S.T.C.), and the Fondation Jacqueline Beytout (B.L.) X.F. was an American Heart Association, Midwest Affiliate, Predoctoral Fellow (grant 13PRE14510056).

■ ABBREVIATIONS USED

UPPS, undecaprenyl diphosphate synthase; FPPS, farnesyl diphosphate synthase; GGPPS, geranylgeranyl diphosphate synthase; CrtM, *S. aureus* dehydrosqualene synthase; MK, menaquinone; MenA, 1,4-dihydroxy-2-naphthoate polyprenyl transferase; MenG, 2-polyprenyl-1,4-naphthoquinone methyltransferase; TMM, trehalose monomycolate; IC_{50}, half maximal inhibitory concentration; MIC, minimum inhibitory concentration required to inhibit the growth of 90% of organisms; PMF, proton motive force; Mt, *M. tuberculosis*; Ms, *M. smegmatis*; Sa, *S. aureus*; Bs, *B. subtilis*; Ec, *E. coli*; Sc, *S. cerevisiae*; Ca, *C. albicans*; Pf, *P. falciparum*; MTT, 3-(4,5-dimethyl-2-thiazolyl)-2,5-diphenyl-2*H*-tetrazolium bromide; IMV, inverted membrane vesicles; TI, therapeutic index; CCCP, *m*-chlorophenylcarbonyl cyanide phenylhydrazone; ACMA, 9-amino-6-chloro-2-methoxyacridine; TLC, thin layer chromatography; THF, tetrahydrofuran

■ REFERENCES

(1) US Department of Health and Human Services Centers for Disease Control and Prevention, Antibiotic resistance threats in the United States 2013. http://www.cdc.gov/drugresistance/threat-report-2013/pdf/ar-threats-2013-508.pdf (accessed March 31, 2014).

(2) World Health Organization, Global tuberculosis report 2013. http://apps.who.int/iris/bitstream/10665/91355/1/9789241564656_eng.pdf?ua=1 (accessed March 31, 2014).

(3) *Report of Two Workshops on Novel Antimicrobial Therapeutics, National Research Council*; The National Academies Press: Washintgon, DC, 2006.

(4) Gray, K. C.; Palacios, D. S.; Dailey, I.; Endo, M. M.; Uno, B. E.; Wilcock, B. C.; Burke, M. D. Amphotericin primarily kills yeast by simply binding ergosterol. *Proc. Natl. Acad. Sci. U.S.A.* **2012**, *109*, 2234−2239.

(5) Fischbach, M. A. Combination therapies for combating antimicrobial resistance. *Curr. Opin. Microbiol.* **2011**, *14*, 519−523.

(6) Silver, L. L. Multi-targeting by monotherapeutic antibacterials. *Nat. Rev. Drug Discovery* **2007**, *6*, 126−126.

(7) Morphy, J. R. The challenges of multi-target lead optimization. *Designing Multi-Target Drugs*; Royal Society of Chemistry: London, 2012; pp 141−154.

(8) Sacksteder, K. A.; Protopopova, M.; Barry, C. E.; Andries, K.; Nacy, C. A. Discovery and development of SQ109: a new antitubercular drug with a novel mechanism of action. *Future Microbiol.* **2012**, *7*, 823−837.

(9) Martin, M. B.; Arnold, W.; Heath, H. T.; Urbina, J. A.; Oldfield, E. Nitrogen-containing bisphosphonates as carbocation transition state analogs for isoprenoid biosynthesis. *Biochem. Biophys. Res. Commun.* **1999**, *263*, 754−758.

(10) Zhang, Y.; Cao, R.; Yin, F.; Hudock, M. P.; Guo, R. T.; Krysiak, K.; Mukherjee, S.; Gao, Y. G.; Robinson, H.; Song, Y.; No, J. H.; Bergan, K.; Leon, A.; Cass, L.; Goddard, A.; Chang, T. K.; Lin, F. Y.; Van Beek, E.; Papapoulos, S.; Wang, A. H.; Kubo, T.; Ochi, M.; Mukkamala, D.; Oldfield, E. Lipophilic bisphosphonates as dual farnesyl/geranylgeranyl diphosphate synthase inhibitors: An X-ray and NMR investigation. *J. Am. Chem. Soc.* **2009**, *131*, 5153−5162.

(11) Protopopova, M.; Hanrahan, C.; Nikonenko, B.; Samala, R.; Chen, P.; Gearhart, J.; Einck, L.; Nacy, C. A. Identification of a new antitubercular drug candidate, SQ109, from a combinatorial library of 1,2-ethylenediamines. *J. Antimicrob. Chemother.* **2005**, *56*, 968−974.

(12) Tahlan, K.; Wilson, R.; Kastrinsky, D. B.; Arora, K.; Nair, V.; Fischer, E.; Barnes, S. W.; Walker, J. R.; Alland, D.; Barry, C. E.; Boshoff, H. I. SQ109 targets Mmpl3, a membrane transporter of trehalose monomycolate involved in mycolic acid donation to the cell wall core of *Mycobacterium tuberculosis*. *Antimicrob. Agents Chemother.* **2012**, *56*, 1797−1809.

(13) La Rosa, V.; Poce, G.; Canseco, J. O.; Buroni, S.; Pasca, M. R.; Biava, M.; Raju, R. M.; Porretta, G. C.; Alfonso, S.; Battilocchio, C.; Javid, B.; Sorrentino, F.; Ioerger, T. R.; Sacchettini, J. C.; Manetti, F.; Botta, M.; De Logu, A.; Rubin, E. J.; De Rossi, E. MmpL3 Is the cellular target of the antitubercular pyrrole derivative BM212. *Antimicrob. Agents Chemother.* **2012**, *56*, 324−331.

(14) Makobongo, M. O.; Einck, L.; Peek, R. M.; Merrell, D. S. *In vitro* characterization of the anti-bacterial activity of SQ109 against *Helicobacter pylori*. *PLoS One* **2013**, *8*, e68917.

(15) SQ109; Global Alliance for TB Drug Development. *Handbook of Anti-Tuberculosis Agents. Tuberculosis*; Elsevier: New York, 2008; Vol. *88*, pp 159−161.

(16) Wallace, R. J., Jr.; Nash, D. R.; Steele, L. C.; Steingrube, V. Susceptibility testing of slowly growing mycobacteria by a microdilution MIC method with 7H9 broth. *J. Clin. Microbiol.* **1986**, *24*, 976−981.

(17) Gale, G. R.; McLain, H. H. Effect of ethambutol on cytology of *Mycobacterium smegmatis*. *J. Bacteriol.* **1963**, *86*, 749−756.

(18) Oldfield, E.; Lin, F. Y. Terpene biosynthesis: Modularity rules. *Angew. Chem., Int. Ed.* **2012**, *51*, 1124−1137.

(19) Meganathan, R. Biosynthesis of menaquinone (vitamin K-2) and ubiquinone (coenzyme Q): A perspective on enzymatic mechanisms. *Vitam. Horm.* **2001**, *61*, 173−218.

(20) Kurosu, M.; Narayanasamy, P.; Biswas, K.; Dhiman, R.; Crick, D. C. Discovery of 1,4-dihydroxy-2-naphthoate prenyltransferase inhibitors: New drug leads for multidrug-resistant gram-positive pathogens. *J. Med. Chem.* **2007**, *50*, 5048−5048.

(21) Kurosu, M.; Crick, D. C. MenA is a promising drug target for developing novel lead molecules to combat *Mycobacterium tuberculosis*. *Med. Chem.* **2009**, *5*, 197−207.
(22) Dhiman, R. K.; Mahapatra, S.; Slayden, R. A.; Boyne, M. E.; Lenaerts, A.; Hinshaw, J. C.; Angala, S. K.; Chatterjee, D.; Biswas, K.; Narayanasamy, P.; Kurosu, M.; Crick, D. C. Menaquinone synthesis is critical for maintaining mycobacterial viability during exponential growth and recovery from non-replicating persistence. *Mol. Microbiol.* **2009**, *72*, 85−97.
(23) Zhang, Y. H.; Cao, R.; Yin, F.; Hudock, M. P.; Guo, R. T.; Krysiak, K.; Mukherjee, S.; Gao, Y. G.; Robinson, H.; Song, Y.; No, J. H.; Bergan, K.; Leon, A.; Cass, L.; Goddard, A.; Chang, T. K.; Lin, F. Y.; Van Beek, E.; Papapoulos, S.; Wang, A. H. J.; Kubo, T.; Ochi, M.; Mukkamala, D.; Oldfield, E. Lipophilic bisphosphonates as dual farnesyl/geranylgeranyl diphosphate synthase inhibitors: An X-ray and NMR investigation. *J. Am. Chem. Soc.* **2009**, *131*, 5153−5162.
(24) Krogh, A.; Larsson, B.; von Heijne, G.; Sonnhammer, E. L. L. Predicting transmembrane protein topology with a hidden Markov model: Application to complete genomes. *J. Mol. Biol.* **2001**, *305*, 567−580.
(25) Kelley, L. A.; Sternberg, M. J. E. Protein structure prediction on the web: A case study using the Phyre server. *Nat. Protoc.* **2009**, *4*, 363−371.
(26) Lin, F. Y.; Liu, Y. L.; Li, K.; Cao, R.; Zhu, W.; Axelson, J.; Pang, R.; Oldfield, E. Head-to-head prenyl tranferases: Anti-infective drug targets. *J. Med. Chem.* **2012**, *55*, 4367−4372.
(27) Valdar, W. S. Scoring residue conservation. *Proteins* **2002**, *48*, 227−241.
(28) Sala, C.; Dhar, N.; Hartkoorn, R. C.; Zhang, M.; Ha, Y. H.; Schneider, P.; Cole, S. T. Simple model for testing drugs against nonreplicating *Mycobacterium tuberculosis*. *Antimicrob. Agents Chemother.* **2010**, *54*, 4150−4158.
(29) Felser, A.; Blum, K.; Lindinger, P. W.; Bouitbir, J.; Krahenbuhl, S. Mechanisms of hepatocellular toxicity associated with dronedarone-a comparison to amiodarone. *Toxicol. Sci.* **2013**, *131*, 480−490.
(30) Garlid, K. D.; Nakashima, R. A. Studies on the mechanism of uncoupling by amine local-anesthetics - evidence for mitochondrial proton transport mediated by lipophilic ion-pairs. *J. Biol. Chem.* **1983**, *258*, 7974−7980.
(31) Moreno-Sanchez, R.; Bravo, C.; Vasquez, C.; Ayala, G.; Silveira, L. H.; Martinez-Lavin, M. Inhibition and uncoupling of oxidative phosphorylation by nonsteroidal anti-inflammatory drugs study in mitochondria, submitochondrial particles, cells, and whole heart. *Biochem. Pharmacol.* **1999**, *57*, 743−752.
(32) Yu, E. W.; McDermott, G.; Zgurskaya, H. I.; Nikaido, H.; Koshland, D. E. Structural basis of multiple drug-binding capacity of the AcrB multidrug efflux pump. *Science* **2003**, *300*, 976−980.
(33) Haagsma, A. C.; Podasca, I.; Koul, A.; Andries, K.; Guillemont, J.; Lill, H.; Bald, D. Probing the interaction of the diarylquinoline TMC207 with its target mycobacterial ATP synthase. *PLoS One* **2011**, *6*, e23575.
(34) Moon, R. B.; Richards, J. H. Determination of intracellular pH by ^{31}P magnetic-resonance. *J. Biol. Chem.* **1973**, *248*, 7276−7278.
(35) Mukkamala, D.; No, J. H.; Cass, L. A.; Chang, T. K.; Oldfield, E. Bisphosphonate inhibition of a Plasmodium farnesyl diphosphate synthase and a general method for predicting cell-based activity from enzyme data. *J. Med. Chem.* **2008**, *51*, 7827−7833.
(36) Bonitz, T.; Alva, V.; Saleh, O.; Lupas, A. N.; Heide, L. Evolutionary relationships of microbial aromatic prenyltransferases. *PLoS One* **2011**, *6*, e27336.
(37) Meng, J.; Wang, F.; Zheng, Y.; Peng, X.; Zhou, H.; Xiao, X. An uncultivated crenarchaeota contains functional bacteriochlorophyll a synthase. *ISME J.* **2009**, *3*, 106−116.
(38) Rao, S. P.; Lakshminarayana, S. B.; Kondreddi, R. R.; Herve, M.; Camacho, L. R.; Bifani, P.; Kalapala, S. K.; Jiricek, J.; Ma, N. L.; Tan, B. H.; Ng, S. H.; Nanjundappa, M.; Ravindran, S.; Seah, P. G.; Thayalan, P.; Lim, S. H.; Lee, B. H.; Goh, A.; Barnes, W. S.; Chen, Z.; Gagaring, K.; Chatterjee, A. K.; Pethe, K.; Kuhen, K.; Walker, J.; Feng, G.; Babu, S.; Zhang, L.; Blasco, F.; Beer, D.; Weaver, M.; Dartois, V.; Glynne, R.; Dick, T.; Smith, P. W.; Diagana, T. T.; Manjunatha, U. H. Indolcarboxamide is a preclinical candidate for treating multidrug-resistant tuberculosis. *Sci. Transl. Med.* **2013**, *5*, 214ra168.
(39) Grzegorzewicz, A. E.; Pham, H.; Gundi, V. A.; Scherman, M. S.; North, E. J.; Hess, T.; Jones, V.; Gruppo, V.; Born, S. E.; Kordulakova, J.; Chavadi, S. S.; Morisseau, C.; Lenaerts, A. J.; Lee, R. E.; McNeil, M. R.; Jackson, M. Inhibition of mycolic acid transport across the *Mycobacterium tuberculosis* plasma membrane. *Nat. Chem. Biol.* **2012**, *8*, 334−341.
(40) Owens, C. P.; Chim, N.; Goulding, C. W. Insights on how the *Mycobacterium tuberculosis* heme uptake pathway can be used as a drug target. *Future Med. Chem.* **2013**, *5*, 1391−1403.
(41) Owens, C. P.; Chim, N.; Graves, A. B.; Harmston, C. A.; Iniguez, A.; Contreras, H.; Liptak, M. D.; Goulding, C. W. The *Mycobacterium tuberculosis* secreted protein Rv0203 transfers heme to membrane proteins MmpL3 and MmpL11. *J. Biol. Chem.* **2013**, *288*, 21714−21728.
(42) Gruppo, V.; Johnson, C. M.; Marietta, K. S.; Scherman, H.; Zink, E. E.; Crick, D. C.; Adams, L. B.; Orme, I. M.; Lenaerts, A. J. Rapid microbiologic and pharmacologic evaluation of experimental compounds against Mycobacterium tuberculosis. *Antimicrob. Agents Chemother.* **2006**, *50*, 1245−1250.
(43) CLSI. Reference Method for Broth dilution Antifungal Susceptibility Testing of Yeasts. In *Approved Standard-Third ed.*; Clinical and Laboratory Standards Institute: Wayne, PA, 2008.
(44) No, J. H.; de Macedo Dossin, F.; Zhang, Y.; Liu, Y. L.; Zhu, W.; Feng, X.; Yoo, J. A.; Lee, E.; Wang, K.; Hui, R.; Freitas-Junior, L. H.; Oldfield, E. Lipophilic analogs of zoledronate and risedronate inhibit Plasmodium geranylgeranyl diphosphate synthase (GGPPS) and exhibit potent antimalarial activity. *Proc. Natl. Acad. Sci. U.S.A.* **2012**, *109*, 4058−4063.
(45) Compain, J. D.; Mialane, P.; Marrot, J.; Secheresse, F.; Zhu, W.; Oldfield, E.; Dolbecq, A. Tetra- to dodecanuclear oxomolybdate complexes with functionalized bisphosphonate. *Chem.—Eur. J.* **2010**, *16*, 13741−13748.
(46) Navon, G.; Ogawa, S.; Shulman, R. G.; Tamane, T. High-resolution ^{31}P nuclear magnetic-resonance studies of metabolism in aerobic *Escherichia coli* cells. *Proc. Natl. Acad. Sci. U.S.A.* **1977**, *74*, 888−891.